Spin Effects Near the Superconductor-Insulator Transition

P.W. Adams

Department of Physics and Astronomy
Louisiana State University
Baton Rouge, LA 70803

Contents

1
Introduction

Ultra-thin metal films have proven to be extraordinarily fertile systems for studying a variety of quantum scattering and interaction processes that ultimately serve to destroy the metallic state of their bulk counterparts (Bergmann, 1983; Dynes *et al.*, 1978). By the early 1980's it was recognized that coherent backscattering in moderately disordered films produces logarithmically insulating behavior at low temperature (Lee and Ramakrishnan, 1985). In addition, disorder tends to enhance the impact of electron-electron ($e-e$) interactions, which manifest themselves as a logarithmic suppression of the density of states near the Fermi energy (Altshuler *et al.*, 1987). The theoretical description of weakly disordered two-dimensional systems has, in fact, been a great success, having given us a quantitative description of a wide spectrum of transport and tunneling density-of-states experiments (Abrahams *et al.*, 1979; Lee and Ramakrishnan, 1985). In contrast, the magnetotransport properties of highly disordered films, with sheet resistance R of the order of the quantum resistance $R_Q = h/e^2$, remain poorly understood (Butko and Adams, 2001). To date there is no clear consensus as to what roles film morphology (Epstein *et al.*, 1983), phase coherent hopping (Nguyen *et al.*, 1985; Entin-Wohlman *et al.*, 1989; Medina *et al.*, 1996), Zeeman splitting (Hernandez *et al.*, 2003; Matveev *et al.*, 1995; Butko *et al.*, 2000*a*), and/or spin-orbit scattering (Shapir and Ovadyahu, 1989; Hernandez and Sanquer, 1992; Pichard *et al.*, 1990) play in producing the correlated insulator phase of ultra-thin metal films. Recently, however, investigators have recognized that new insights into the processes that contribute to the formation of the correlated insulator phase can be obtained through the study of metal films that undergo a superconductor-to-insulator (S-I) transition (Goldman and Markovic, 1998). The reason for this is obvious. On the one hand, superconductors are characterized by a macroscopic quantum state which exhibits long range phase coherence and non-dissipative current flow. Insulators, on the other hand, have no long range coherence of any sort and exhibit dissipative, glassy dynamics. The fact that this striking juxtaposition of electronic properties can be controlled via an external tuning parameter, such as film resistance, allows one to explore the emergence of the insulating phase from the perspective of the superconducting phase and its attendant fluctuations.

In practice, a superconducting film can be driven into the insulating phase by increasing its disorder beyond a specific threshold. Typically this is done by making the film thinner, and, once the normal state sheet resistance is of the order of R_Q, the superconducting phase gives way to a highly insulating phase (Haviland *et al.*, 1989). Alternatively, if the system is close to the insulating threshold, a magnetic field can be used to tune the system through the S-I transition (Hebard and Paalanen,

1990). The S-I transition has been the subject of intense investigation for more than two decades now. The primary interest has been in those systems which are homogeneously disordered and, in particular, non-granular. It is generally believed that the disorder-driven SI transition in these systems is mediated by $e-e$ interaction effects (J. M. Valles *et al.*, 1992). With increasing disorder, an otherwise perturbative depletion of quasiparticle states at the Fermi energy grows into a full-blown correlation gap when $R >> R_Q$ (Butko *et al.*, 2000*b*; Butko and Adams, 2001). This has the effect of undermining the superconducting order parameter amplitude, thereby suppressing the transition temperature T_c (J. M. Valles *et al.*, 1992). However, the exact nature of the insulating state, and its relation to the superconducting phase, remains unclear. For instance, anomalously large, multi-fold, negative magnetoresistances have been reported in ultra-thin TiN films (Baturina *et al.*, 2007), InO_x films (Gantmakher *et al.*, 1998; Gantmakher *et al.*, 2000; Steiner *et al.*, 2005) and in insulating Be (Butko *et al.*, 2000*b*) films. The MR of these films saturates at a weakly temperature dependent resistance that is always near R_Q, *i.e.* the "quantum metal" phase (Baturina *et al.*, 2007; Butko and Adams, 2001). This observation suggests that the zero-field insulating ground state is distinctly different from the high-field ground state, which has led to speculation that the zero-field ground state has an incoherent superconducting component (Sambandamurthy *et al.*, 2004; Stewart *et al.*, 2007).

Though the S-I transition has been studied extensively over the last 30 years, there are, in fact, very few experiments that have directly probed the spin degrees of freedom of the system in the region near the zero-field transition. Several conditions must be met for one to probe spin effects in thin disordered films. First, the film must have a relatively low intrinsic spin-orbit scattering rate (SOS). Otherwise, the spin-orbit interaction will mix the spin-up and spin-down eigenstates, and spin will no longer be a good quantum number. Second, one must find a way to couple to the spin moments without coupling to the orbital degrees of freedom. In practice, the is done through the Zeeman splitting from an applied magnetic field. If a film is very thin, i.e. thinner than the diffusion length and/ or the superconducting coherence length, then the orbital response can be effectively suppressed by aligning the plane of the film parallel to the applied field. Third, one needs a microscopic probe that is sensitive to spin, such as electron tunneling.

Numerous spin studies of ultra-thin Be and Al films have shown that these light elements have a very low intrinsic SOS rate (Tedrow and Meservey, 1979; Adams, 2004; Adams *et al.*, 1998) and are true spin-singlet superconductors. Here we will review the spin properties of these systems on either side of the zero-field superconductor-insulator transition. We will begin with an overview of high field superconductivity in thin, moderately disordered Al and Be films with an emphasis on their spin degrees of freedom. Next we will consider the magnetotransport properties of homogeneously disordered Be films that are on the insulating sided of the S-I transition. Of course, our ultimate goal is to use spin to probe the quantum characteristics of the zero-field S-I transition.

2
The Parallel Field S-I Transition

2.1 The Spin-Paramagnetic Transition

Magnetic fields generally have a detrimental effect on superconductors via two independent channels. The first is an orbital effect associated with the fact that cyclotron motion is incompatible with the formation of Cooper pairs and hence superconductivity; for the vast majority of superconducting systems the critical field transition is completely dominated by the orbital response of the conduction electrons. The second channel is the Zeeman coupling to the electron spin. This Zeeman splitting can be made the dominant pairbreaking mechanism by inhibiting the orbital response. This is typically done by applying a magnetic field in the plane of a superconducting film whose thickness t is much less than the superconducting coherence length ξ and whose electron diffusivity is low (Fulde, 1973; Meservey *et al.*, 1970; Wu and Adams, 1994). Under these conditions the phase transition to the normal state is mediated by the spin polarization of the electrons, and near the critical field the electron Zeeman splitting is of the order of the superconducting gap energy. A first-order transition from the superconducting state to the paramagnetic normal state occurs at the Clogston-Chadrasekhar critical field (Clogston, 1962; Chandrasekhar, 1962)

$$H_c^{CC} = \frac{\Delta_o \sqrt{1+G^0}}{\sqrt{2}\mu_B} \tag{2.1}$$

where Δ_o is the zero-field, zero-temperature gap energy; μ_B is the Bohr magneton; and G^0 is the antisymmetric Fermi-Liquid parameter. Note that, if Δ_o is known, then by Eq. 2.1, the parallel critical field of a thin film gives a direct measure of G^0, assuming spin-orbit effects are negligible. G^0 affects the spin response of the system and is related to the ratio of the spin susceptibility density of states $N(\chi)$ to the heat capacity density of states $N(\gamma)$ by $G^0 = N(\gamma)/N(\chi) - 1$ (Baym and Pethick, 1991).

Though G^0 is a fundamentally important parameter in the many-body description of metals, there have been very few measurements of it reported in the literature. This is due, in part, to the fact that it is exceedingly difficult to measure it directly in bulk systems. To date, measurements of G^0 have been extracted from high-field tunneling density of states (DOS) and critical field studies of low atomic mass superconducting films. Estimates of normal state value of G^0 have been reported via tunneling studies of the Zeeman splitting of the BCS density of states in superconducting Al films, $G^0 \sim 0.3 - 0.4$, (Alexander *et al.*, 1985; Tedrow *et al.*, 1984) in the intermediate temperature regime where the superconducting order parameter is partly suppressed by thermal fluctuations. Low temperature DOS measurements in amorphous Ga films,

which is a strong coupling superconductor, give a somewhat larger value of $G^0 \sim 0.81$ (Gibson *et al.*, 1989). Alternatively, G^0 can be extracted from parallel critical field measurements. This method gives $G^0 \sim 0.23$ in TiN films (Suzuki *et al.*, 2000). The only direct measurements of G^0 have been obtained in the normal state, via the field dependence of the pairing resonance (Aleiner and Altshuler, 1997) in Al, $G^0 \sim 0.17$,(Butko *et al.*, 1999) and Be films, $G^0 \sim 0.21$ (Adams and Butko, 2000). In all these systems the spin-orbit scattering is quite low, thus spin remains a good quantum number.

2.2 Parallel Field Studies of Ultra-Thin Al and Be Films

2.2.1 Thin Film Synthesis and Characterization

In thin metal films the SO scattering rate, $1/\tau_{so}$, increases with increasing atomic mass Z as $\tau_s/\tau_{so} \sim Z^4$, where τ_s is the surface scattering time (Meservey and Tedrow, 1976), suggesting that light elemental films are the best candidates for purely spin singlet superconductivity. Indeed, extensive studies of the parallel critical field transition, commonly known as the spin-paramagnetic (S-P) transition, in Al and Be films have shown that the characteristic spin-orbit scattering rate in these elements is very low. Aluminum films tend to form a granular microstructure, but very thin Be films can be made with a smooth, dense, homogeneously disordered, microstructure. Al (Be) films used in S-P studies are typically made by e-beam deposition of 3 - 5 nm of 99.999% Al (99.5%Be) onto fire polished glass microscope slides cooled to 84 K. Usual deposition rates are $\sim$ 0.1 nm/s in a vacuum of $\sim$ 0.5 μTorr. The Al (Be) films have a transition temperature $T_c \sim 2.7$ K ($T_c \sim 0.5$ K) and a parallel critical field $H_{c||} \approx 6.0$ T ($H_{c||} \approx 1.0$ T). Tunnel junctions are formed by exposing the films to atmosphere for $0.2 - 1$ hours in order to form a native oxide. Then a strip of metal is deposited on the upper surface of the film at 84 K to form a tunneling counter-electrode. The counter-electrode can either be a non-superconducting material such as Ag or a relatively thick ($t > 7$ nm) strip of Al which will have a low parallel critical field. At low temperatures the tunneling conductance is proportional to the product $N_{ce}N_{film}$, where N is the quasiparticle density of states. Since the counter-electrode DOS is independent of energy, the tunneling conductance gives a direct measure of the superconducting film DOS. Alignment with the external field is crucial in these experiments, so alignment must be made with an *in situ* mechanical rotator.

2.2.2 S-P Phase Diagram

Low temperature measurements of the tunneling conductance as a function of parallel magnetic field reveal that the tunneling spectrum of thin Al and Be films changes abruptly at the critical field and displays a surprisingly large hysteresis. The hysteresis is a consequence of the first-order nature of the critical field transition. The most complete studies of the hysteretic S-P transition have been made on Al films, which will be the primary focus of this section. In Fig. 2.1 the zero-bias tunnel junction conductance G(0) is plotted as a function of parallel field at the critical field transition of a 1 kΩ/sq Al film. The precipitous attenuation in G(0) as the field is lowered through the transition is due to the sudden opening of the superconducting gap in the single

particle DOS. As a consequence there is an exponential suppression of the zero bias tunnelling conductance (Tinkham, 1996).

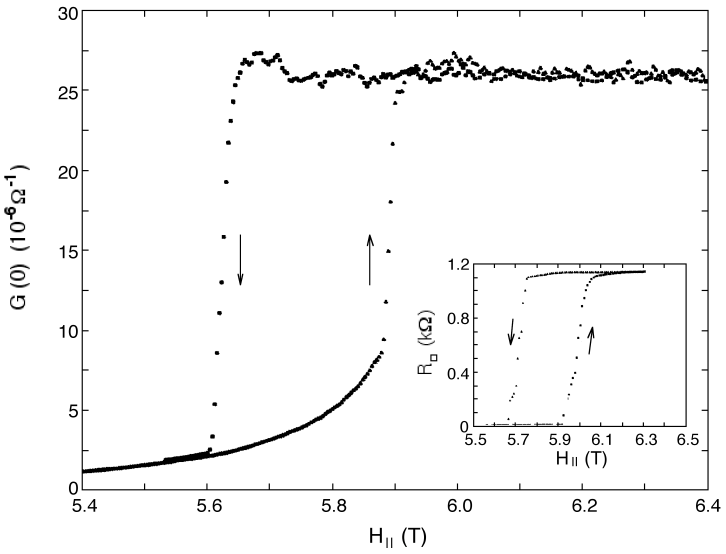

Fig. 2.1 Hysteresis in zero-bias tunneling conductance as a function of parallel field for a 3 nm-thick Al film at 30mK. Arrows depict field sweep direction. Inset: corresponding hysteresis in film sheet resistance.

The hysteresis in the DOS indicates that the non-equilibrium aspects of the transition are intrinsic to the superconducting condensate itself. In Fig. 2.2 a phase diagram is produced by plotting the up-sweep and downsweep critical fields as a function of temperature, where the critical field is defined by the onset of a gap in zero bias tunneling conductance, G(0). Note that the hysteresis opens up below the tricritical point temperature $T_{Tri} \sim 0.6$ K. A similar phase diagram has been reported for Be films.

The dashed lines in Fig. 2.2 are provided to help the reader visualize the field and temperature cycles used to explore the phase diagram. Indeed, Fig. 2.2 represents the classic S-P phase diagram in which a high-temperature line of second-order phase transitions terminates into a line of first-order transitions at the tricritical point $T_{tri} \sim 0.3T_c$. The low-temperature superconducting S and normal N phases are separated by a robust coexistence region in which the state of the system is solely determined by the system state prior to entering the region, i.e., the state memory SM region. If one were to start from the high field, low temperature point a in the normal state and then lower the field to point c, just above the lower critical field branch, then the system would be in metastable normal state. This 'glassy' normal state can be melted by simply cutting across the diagram $c \rightarrow e$, thereby inducing superconductivity via

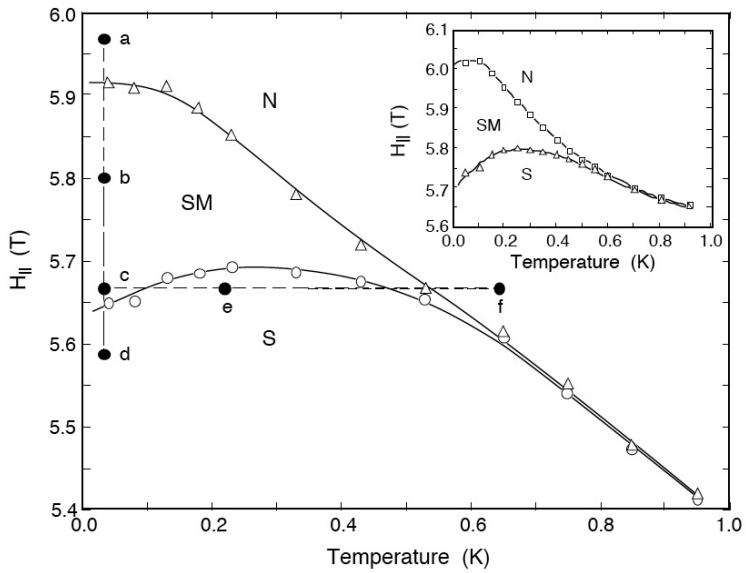

Fig. 2.2 Parallel critical fields as a function of temperature as measured by the zero bias tunnel junction conductance. Triangles refer to up-sweep transitions and circles to down-sweep transitions. The letters and dotted lines are provided as a guide to the field and temperature cycles discussed in the text. S: Superconducting phase. N: Normal phase. SM: State memory region. Inset: Parallel critical fields as measured by resisitive transitions.

warming. Similarly, a metastable superconducting state can be formed by moving from $d \rightarrow b$. The precise role disorder and microspcopic morphology play in determining the details of the phase diagram are unknown. However, it is evident that the first order S-P transition is intrinsically hysteretic, and films that are near the SM region exhibit glassy, non-equilibrium dynamics (Wu and Adams, 1995).

2.3 High Field Spin-Resolved Tunneling

2.3.1 Superconducting Phase

One of the most striking consequences of spin rotation symmetry is the field-induced modification of the BCS density of states spectrum due to the Zeeman interaction. Under the same conditions that give rise to the first order S-P transition, one finds that, in a subcritical parallel field, the BCS quasiparticle coherence peaks are split into spin-up and spin-down subbands, as is shown in Fig. 2.3. This effect was first reported by Tedrow and Meservey, who would later go on to use it as spin-resolved tunneling probe of thin magnetic films. The BCS peaks are separated by the Zeeman energy. Spectra such as this provide irrevocable evidence that spin is a good quantum number in Al and Be films. Note that, with increasing field, the innermost peaks move toward the Fermi energy (*i.e.* V=0). However, by Eq. 2.1 the critical field will be crossed before the spin-up and spin-down sub-bands overlap.

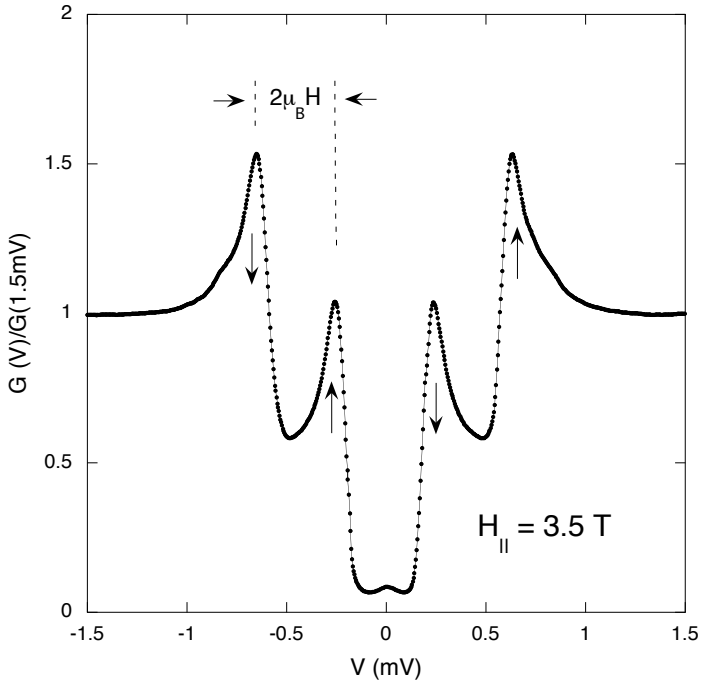

Fig. 2.3 Tunneling conductance of of 26 Å superconducting Al in a parallel field of 3.5 T. Note the Zeeman splitting of the BCS density of states. The arrows denote the spin assignments of the peaks.

2.3.2 Pauli-limited Normal State

The spin symmetry of ultra-light superconductors is not only manifested in the S-P transition itself but also in the Pauli-limited paramagnetic normal state, as well (*i.e.* $H > H_{c||}$). In particular, an unexpected pairing resonance, clearly associated with virtual Cooper pair formation, was discovered in the paramagnetic DOS spectrum of Al and Be films (Wu *et al.*, 1995; Adams and Butko, 2000) in the mid 1990's. Shown in Fig. 2.4 are typical 60 mK tunneling spectra of a 2.6 nm thick Al film in several parallel fields above $H_{c\|}$. The spectra display a logarithmic depletion of states near the Fermi energy, commonly known as the zero bias anomaly (ZBA). It is now well established that the logarithmic ZBA, which is independent of field, is associated with electron-electron interactions in two-dimensional (2D) disordered systems (Altshuler *et al.*, 1987). Indeed, the magnitude of the ZBA grows rapidly with increasing film resistance, and in films with $R \sim R_Q$ the depletion can be sufficiently extensive so as to undermine the formation of superconducting condensate.

The satellite features in Fig. 2.4 are due to the pairing resonance and represent a window into the processes that ultimately lead to the formation of stable Cooper pairs

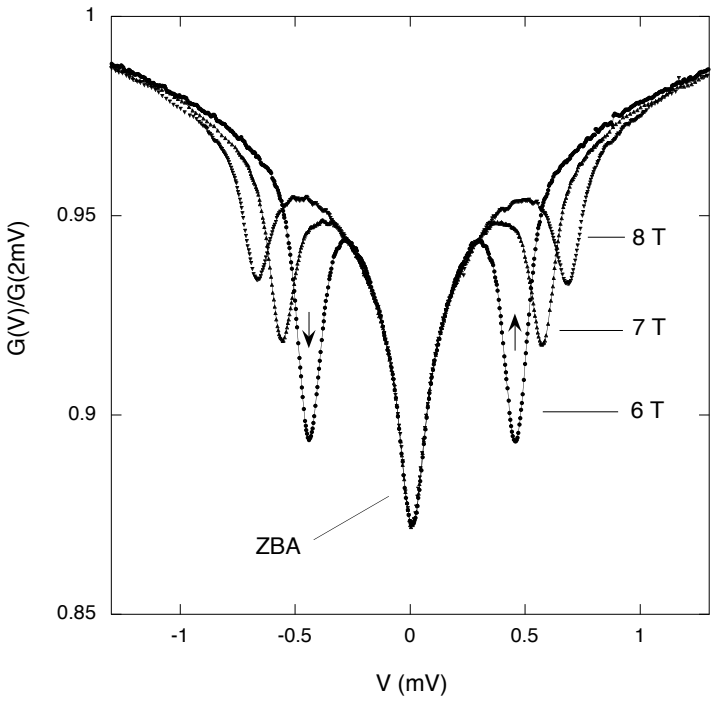

Fig. 2.4 The T = 70 mK normal state tunneling conductance at several supercritical parallel magnetic fields in a 2.6 nm-thick Al film with sheet resistance $R \sim 1$ kΩ. The central feature is the zero bias anomaly (ZBA), which is an electron-electron interaction effect. The satellite features represent the pairing resonance. The arrows denote the spin assignments of the occupied and unoccupied resonances.

at lower fields. Figure 2.5 shows the resonance in a 2.3 nm thick Be film with $T_c \sim 0.6$ K. The resonance can be observed in high field tunneling by virtue of the fact that it is a spin-singlet mode riding on top of a paramagnetic background. The spin structure of the resonance is depicted in Fig. 2.6, which shows an idealized tunnel junction between a non-superconducting paramagnetic counter-electrode (PM) and the Pauli-limited normal state (PLNS) of a superconducting film in a supercritical parallel magnetic field. The discrete momentum states near the Fermi energy are singly occupied, as shown in Fig. 2.6 where $E_z = g_L \mu_B H$ is the Zeeman energy, and $g_L = 2/(1 + G^0)$ is the renormalized Landé g-factor.

The pairing resonance is associated with evanescent Cooper pairs formed via the two tunneling channels indicated by the forward and reverse bias arrows. In particular, at the appropriate bias a doubly occupied electron (hole) state is formed, which then mixes with the nearby unoccupied electron (hole) states lying above (below). This mixing results in a virtual Cooper pair, which in turn depletes single particle states in

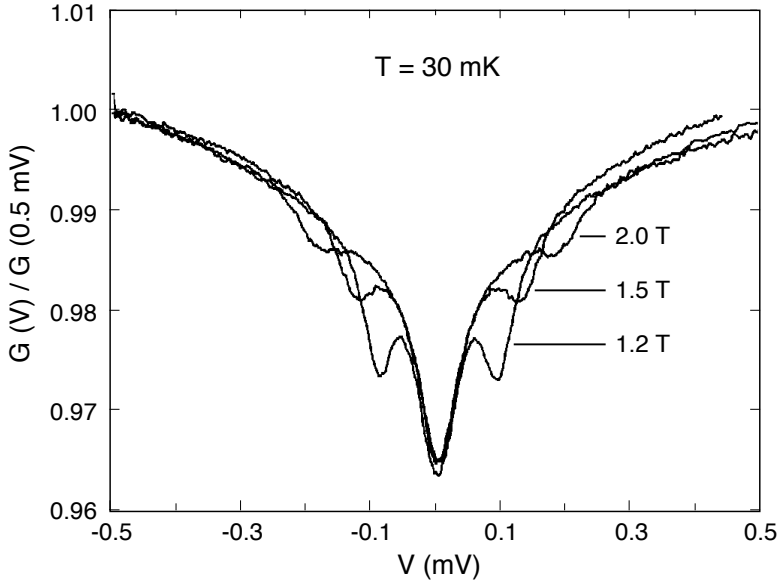

Fig. 2.5 The pairing resonance in a 2.3 nm thick Be film with $T_c = 0.55$ K and $R = 260\ \Omega$.

the vicinity, hence the dips in the spectra of Figs. 2.4 and 2.5. Though the resonance lies near the Zeeman voltage $V_z = E_z/e$, its precise energy is determined, in part, by the potential energy of the Cooper pair . Using a nonperturbative approach, Altshuler *et. al.* (Aleiner and Altshuler, 1997) showed that the resonance occurs at an energy that is universal for 0D(grain), 1D(wire), and 2D(film) systems,

$$V^* = \frac{1}{2}\Big[V_z + \sqrt{V_z^2 - (\Delta_o/e)^2}\Big], \tag{2.2}$$

where $V_z = E_z/e$. As can be seen in Fig. 2.7, Eq. 2.2 is in reasonably good agreement with parallel field measurements in Al and Be films. The solid lines are least-squares fits to Eq. 2.2 in which only g_L was varied. Recently, it has been shown that by fitting the resonance profile to theory one can obtain quite accurate estimates of virtually all of the relevant superconducting microscopic parameters, Δ_o, the spin orbit scattering rate $1/\tau_{so}$, G^0, and the elastic scatter rate $1/\tau_o$.

Up to now the PR has been primarily studied in relatively low resistance Al films, $R < R_Q/4$. Clearly, however, one would like to follow its evolution as the zero-field superconductor-insulator (S-I) transition is approached. It is now generally accepted that, for sufficiently strong disorder, the order parameter in a non-granular superconducting film will be destroyed by the repulsive $e-e$ interactions that give rise to the ZBA. Insights into this process could, in principle, be obtained by comparing the superconducting gap amplitude with the strength of the pairing resonance as one increases the resistance to values near R_Q. Since the resonance lies well above the Fermi

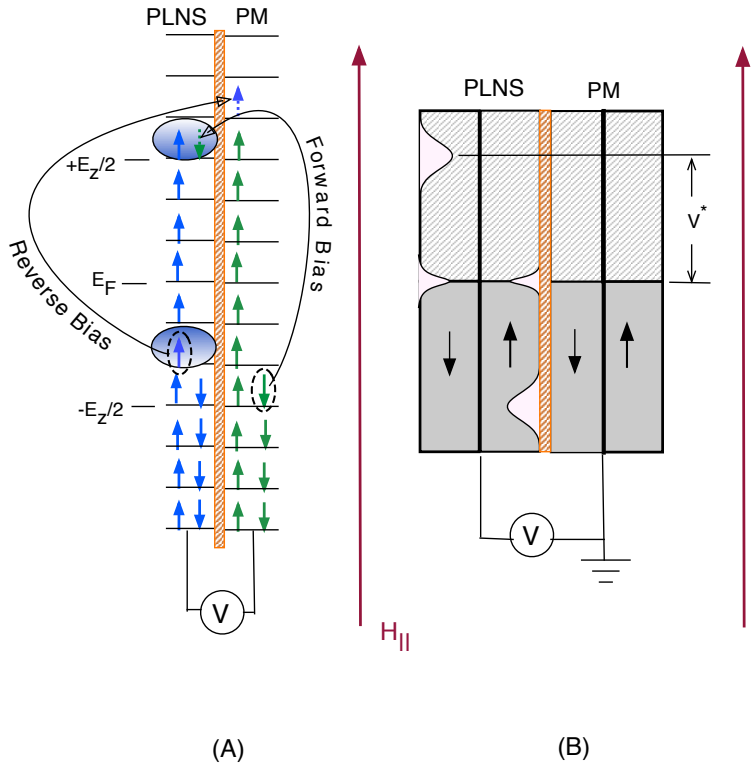

Fig. 2.6 A: Schematic of a tunnel junction between the Pauli-limited normal state (PLNS) of a superconducting film in a supercritical parallel magnetic field and a paramagnetic (PM) non-superconducting metal. Note that the Zeeman splitting results in singly occupied orbitals near the Fermi energy. By applying a voltage, the states on either side of the junction can be shifted relative to each other. The diagram shows the tunneling channel that produces the relevant singlet electron state in forward bias and the corresponding singlet hole state in reverse bias. These singlet states resonantly mix with nearby empty states thereby forming evanescent Cooper pairs. B: DOS profiles of a tunnel junction comprised of an Al film in the PLNS on one side and a paramagnetic film on the other. Note the depletion of states in the PLNS due to the pairing resonance and the zero bias anomaly.

energy, it may survive on the insulating side of S-I transition by virtue of the fact that it is shifted away from the $e-e$ correlation singularity at $V = 0$. Interestingly, in moderately disordered films the resonance deepens with increasing film resistance because resonant electron pairs with lower diffusivity spend more time interacting. Of course, the same is true in the repulsive interaction channel, which results in a deepening of the ZBA.

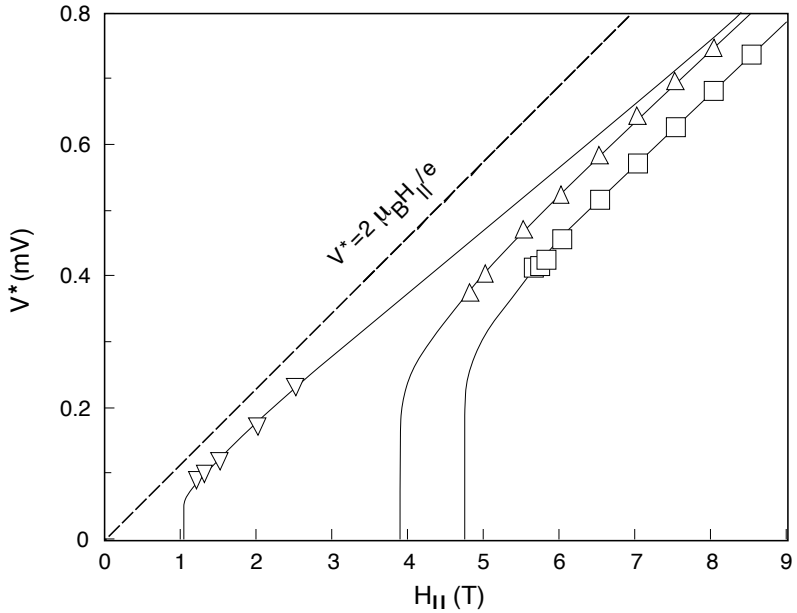

Fig. 2.7 Voltage position of the PR as a function of parallel magnetic field. Squares: $\Delta/e = 0.45$ mV Al film; Up triangles: $\Delta/e = 0.38$ mV Al film; Down triangles: $\Delta/e = 0.1$ mV Be film. The dashed line is the Zeeman voltage with $g_L = 2$. The curved lines are least square fits of Eq. 2.2 to the data in which g_L was varied.

3
Spin Effects in the Insulating Phase

3.1 Introduction and Background

Here we will review the magneto-transport and tunneling density of states properties of ultra-thin, homogeneously disordered Be films that are on the insulating side of the zero field S-I transition. Be films with $R \ll R_Q$ are typically superconducting with $T_c \sim 0.5 - 3$ K depending on the details of the deposition parameters. However, if one descreases the film thickness to the point where $R \sim R_Q$, then the superconducting phase gives way to a highly correlated, variable range hopping, phase. The relationship between the insulating ground state and the superconducting ground state on either side of the S-I transition remains the subject of intense experimental and theoretical work. A growing body of evidence suggests that localized Cooper pairs play an important role in the formation of the insulating ground state. For our purposes here it is best to begin with an overview of the theory of interaction effects in disordered electronic systems which neglects the possibility of localized Cooper pairs. From this vantage we can consider recent experimental results within the context of the standard localization formalism in order to assess the need for more exotic models. Localization theory has for the most part been developed in two extreme limits. In the weak disorder/interaction 2D limit, it is well established that the primary effect of $e-e$ interactions is to produce a logarithmic suppression of the DOS at the Fermi energy (Altshuler *et al.*, 1987), $\delta N \sim -\ln(V)$. This is manifest as the ZBA and has been well established in a number of different systems via tunneling measurements of the DOS (Imry and Ovadyahu, 1982; White *et al.*, 1985). The depletion of the DOS is perturbative and results in a weakly metallic $\ln T$ transport conductivity [2]. In the opposite limit, i.e., strongly insulating regime, Efros and Shklovskii (Efros and Shklovskii, 1984; Efros and Shklovskii, 1975) have shown that the Coulombic interactions can produce a nonperturbative gap in the DOS, which is commonly known as the Coulomb gap (Massey and Lee, 1995). Interestingly, the 2D Coulomb gap is expected to be linear in energy (Efros and Shklovskii, 1984),

$$N(eV) = \frac{\alpha(4\pi\epsilon_o\kappa)^2|eV|}{e^4} \tag{3.1}$$

where κ is the relative dielectric constant, ϵ_o is the permittivity of free space, and α is a constant of order unity. The Coulomb gap is usually associated with a modified variable range hopping law of the form in the transport characteristics

$$R(T) = R_o \exp(T_o/T)^\nu \tag{3.2}$$

where R is the film sheet resistance and R_o is a constant. In the case of a flat DOS near the Fermi energy, the transport simply obeys Motts variable range hopping law with $\nu = 1/3$ (Mott and Davis, 1979). If there is a simple gap in the DOS then T_o is the gap energy for fixed range hopping and $\nu = 1$. Finally, if the DOS spectrum is given by Eq. 3.1, then one expects $\nu = 1/2$, R_o to be of the order of the quantum resistance R_Q (Efros and Shklovskii, 1984), and

$$T_o = \frac{2.8e^2}{4\pi k_B \epsilon_o \kappa \xi} \tag{3.3}$$

where k_B is the Boltzmann constant and ξ is the localization length. Thus, when the $\nu = 1/2$ hopping form is observed, the DOS spectrum is simply assumed to be that of Eq. 3.1. Below we examine this assumption through a systematic electron tunneling DOS study of uniformly disordered Be films whose transport properties range from that of weakly metallic to strongly insulating.

3.2 Insulating Be Films

Beryllium forms smooth, dense, nongranular films when thermally evaporated onto glass. In fact, scanning force micrographs of the films exposed oxide surface do not reveal any salient morphological features down to a resolution of 0.5 nm. This nongranular morphology is crucial in that it assures one that the measured resistance is representative of $e - e$ correlation processes and not those associated with grain charging. In extremely high resistance films any significant granularity will result in field-independent grain charging (Coulomb blockade) effects which preempt the many body effects of interest. The Be films used in these studies ranged in thickness from $1.5 - 2.0$ nm, with corresponding sheet resistances $R \sim 500\ \Omega - 3\ \mathrm{M}\Omega$ at $T = 50$ mK. They were deposited by thermally evaporating 99.5% pure beryllium powder onto fire polished glass substrates held at 84 K. The evaporations were made in a 0.4 μTorr vacuum at a rate 0.30 nm/s. The film area was 1.5 mm x 4.5 mm. Transmission electron microstructural analysis of 15 nm thick Be films deposited on cleaved NaCl crystals at 84 K revealed that the films were composed of an ultrafine base structure that was interspersed with $5 - 15$ nm Be nanocrystallites. Electron diffraction measurements showed no diffraction from the metallic base structure suggesting that it was amorphous. Similarly the oxide (BeO) produced a broad, continuous diffraction ring indicating its grain size was less than 1 nm (Adams *et al.*, 1998).

3.3 Variable Range Hopping and the Coulomb Gap

Shown in the inset of Fig. 3.1 is the normal state conductance of the 2600 Ω film as a function of $\ln T$. This sample had a superconducting transition temperature $T_c = 0.33$ K which was suppressed by the application of a magnetic field. The film exhibited the expected $\ln T$ weakly insulating behavior with some rounding below 100 mK. In stark contrast, the main body of Fig. 3.1 shows the activated-like behavior of a 2.6 MΩ film. The solid line is a least squares fit to the data. The linearity of the data in Fig. 3.1 shows unequivocally that the hopping exponent is $\nu = 1/2$. Furthermore the slope and intercept of the fit determine the parameters $T_o = 1.6$ K and $R_o \sim R_Q/2$ in Eq. 3.2.

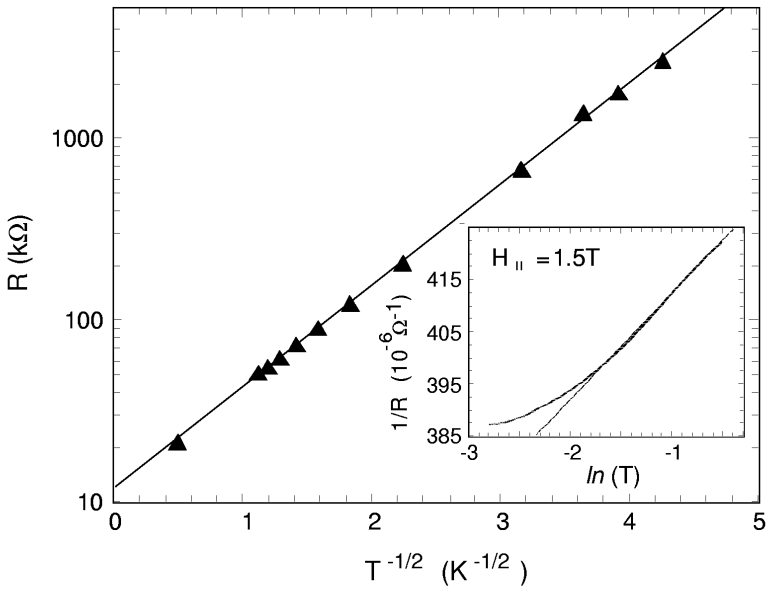

Fig. 3.1 Semilog plot of the resistance of a 2.6 MΩ Be film as a function of $T^{-1/2}$. The solid line is a linear fit to the data for which we get $T_o = 1.6$ K and $R_o = h/2e^2$. Inset: Conductance of a 2600 Ω film as a function of $\ln T$. The solid line is a guide to the eye.

In principle we can use Eq. 3.3 along with the measured value of T_o to calculate a localization length ξ. However, the relative dielectric constant κ in Eq. 3.3 is unknown for a highly disordered metal film. Alternatively, if one instead assumes that $\xi \sim 1$ nm and takes $T_o = 1$ K, then Eq. 3.3 gives $\kappa \sim 10^4$. This value seems reasonable in that it lies between the metallic and insulating limits of $\kappa \sim \infty$ and $\kappa \sim 10$, respectively. This is not an issue in 3D semiconducting systems where the dielectric constant is well defined in the insulating phase. In any case, it is evident that Fig. 3.1 is consistent with the existence of the Coulomb gap described by Eq. 3.2.

In Fig. 3.2 we show the evolution of the tunneling DOS of thin Be films as the sheet resistance is increased from a few hundred ohms to several megaohms. We note that the DOS spectrum of the lowest resistance film in this plot displays a logarithmic ZBA, as expected. However, the magnitude of the ZBA feature grows rapidly with increasing disorder. Indeed, in films with $R > 10^4\Omega$ the spectrum is no longer perturbative, and no longer logarithmic in form. Deep in the insulating phase, the energy dependence of the DOS spectrum becomes linear as can be seen in the 2.6 MΩ film. This linear dependence is predicted by Eq. 3.1 and represents the 2D Coulomb gap.

3.4 Multi-fold Magnetoconductance and Quantum Metallicity

Though the data in Figs. 3.1 and 3.2 are consistent with standard descriptions of modified variable range hopping, the application of magnetic field shows that the

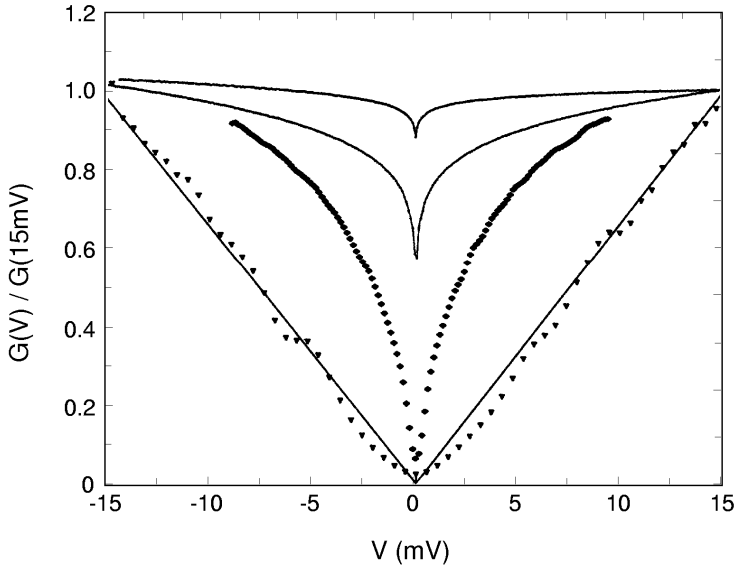

Fig. 3.2 Tunneling conductances normalized to $G = 15$ mV for Be films with $T = 50$ mK resistances of $R = 530\ \Omega$, 2.6 kΩ, 16 kΩ, and 2.6 MΩ (top to bottom). The solid lines are a best fit to the form $G(V) = b|V|$, where b is an adjustable parameter. The 2.6 MΩ data was taken at 700 mK; the other curves were measured at 50 mK.

underlying quantum state of high resistance films is, in fact, anomalous. Plotted in Fig. 3.3 is the magnetoconductance (MC) of a 3 MΩ Be film at 50 mK with field applied perpendicular and parallel to the film surface. Below ~ 1 T the MC of the film is negative, with the conductance falling about a factor of two. Above 1 T the MC is positive and linear for both field orientations. The magnitude of the MC is a function of the film disorder. In the inset of Fig. 3.3 we show a similar, but much smaller, MC in a 16 kΩ film.

The overall magnitude of the MC data in Fig. 3.3 is extremely large and cannot easily be explained within the framework of variable range hopping theory. Assuming that the parallel field MC is entirely mediated by the Zeeman interaction, it is clear from the data that the orbital and spin contributions to the MC are comparable. In Fig. 3.4 we show that the $T^{-1/2}$ VRH behavior is preserved in parallel field, and that the primary effect of the field is to diminish the correlation energy T_o. Again, this is not easily explained in the context of standard strong localization theory.

The positive MC in the main panel of Fig. 3.3 shows no sign of saturation, up to the highest fields studied. Naturally, one would expect the MC to saturate on field scales in which the correlation energy T_o is driven to zero. In order to address this issue we present magnetoresistance (MR) data on Be films with substantially lower disorder than the films in Fig. 3.3. Shown in Fig. 3.5 is the temperature dependence of the film resistance normalized by R_Q for two critically disordered samples in zero field and at

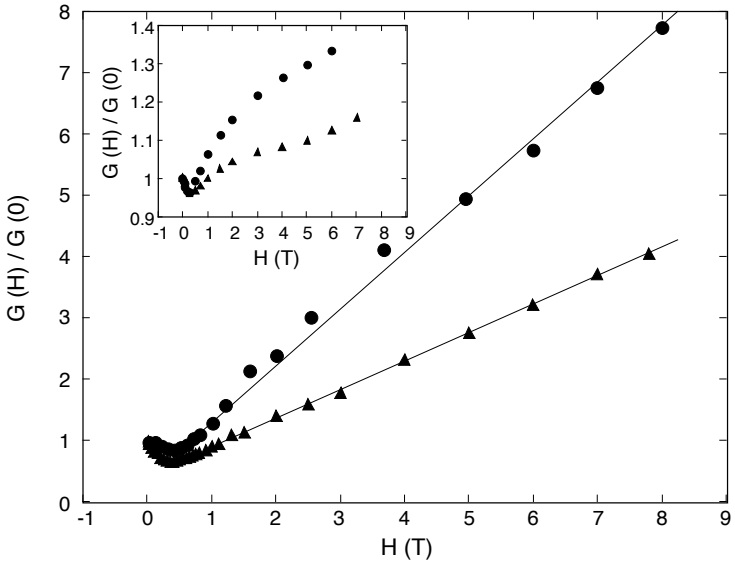

Fig. 3.3 Relative magnetoconductance of a 3 MΩ Be film at 50mK. Circles: field perpendicular to film surface. Triangles: field parallel to film surface. The solid lines are linear fits to the data above 1 T with slopes of 1/(1.1T) and 1/(2.2T) for the perpendicular and parallel data respectively. Inset: relative magnetoconductance of a 16 kΩ Be film.

8.4 T respectively. The zero field data are strongly insulating, but the high field data appear to be more metallic in character. Obviously the magnetic field is producing a significant suppression of the insulating phase. This is also evident in Fig. 3.6 where we show the low temperature MR of the films. Note that the low field MR is positive, but above 1 T the MR becomes strongly negative. The overall structure of the data in Fig. 3.6 is consistent with the MR behavior of highly insulating films of Fig. 3.3 with the notable exception of the provocative saturation of the MR to the quantum resistance.

MR peaks and anomalously large, multi-fold, negative magnetoresistances have also been reported in ultra-thin TiN films (Baturina *et al.*, 2007), and InO_x films (Gantmakher *et al.*, 1998; Gantmakher *et al.*, 2000; Steiner *et al.*, 2005). In a fashion similar to the data in Fig. 3.6 the MR of these films saturates at a weakly temperature dependent resistance that is always near R_Q, suggesting the existence of a high-field "quantum metal" phase (Baturina *et al.*, 2007; Butko and Adams, 2001). These experiments provide strong evidence that the zero-field insulating ground state is distinctly different from the high-field ground state. This has led to speculation that the zero-field ground state has an incoherent superconducting component (Sambandamurthy *et al.*, 2004; Stewart *et al.*, 2007) that mediates the insulating behavior.

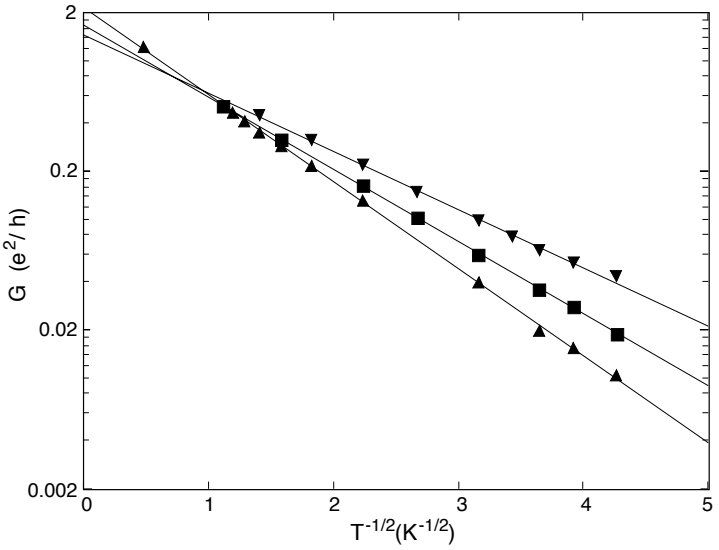

Fig. 3.4 Semi-log plot of the film conductance as function of $T^{-1/2}$ at three different parallel magnetic fields. Up triangles: $H_{||} = 0$. Squares: $H_{||} = 3.0T$. Down triangles: $H_{||} = 7.0T$. The solid lines are linear fits to the data from which $T_o(H_{||})$ were obtained via Eq. 3.2.

.

3.5 Quantum Metallicity and Spin-Orbit Scattering

Interestingly, both Be and TiN films form dense homogeneously disordered, non-granular films with an intrinsic, clean limit, $T_c \sim 1$ K. As we discuss below, the fact that both of these systems have a well documented, low SOS rate is crucial to the observation of the quantum metal phase. If the insulating side of the S-I transition in Be, TiN, and InO_x films is mediated by localized Cooper pairs, i.e. a Bose insulator, then one should be able to probe the local condensate with magnetic field. In particular, assuming that parallel magnetic field acts only on the electron spins, then the MR of the Be films can be attributed to the Zeeman splitting of the localized Cooper pairs. This is analogous to the S-P mechanism in the superconducting phase. Since the Zeeman-mediated critical field of low SOS superconductors is simply proportional to the superconducting gap (Wu *et al.*, 2006), it is natural to assume that the local pair-breaking field in the insulating phase will also be proportional to the local energy gap. To account for the field range over which MR is significant, one must assume that there is a rather broad distribution of local pair binding energies. In the presence of SOS the Zeeman critical field of a superconductor can be much larger than that of the zero-SOS case. Beryllium and Al films have a very low intrinsic SOS rate (Tedrow and Meservey, 1979; Adams, 2004; Adams *et al.*, 1998), but a controllable amount of SOS can be induced in thin these films by coating them with heavy noble

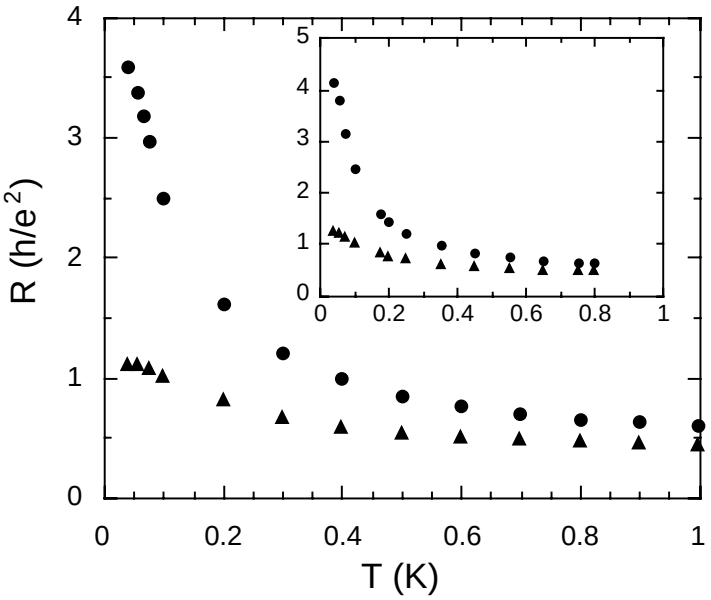

Fig. 3.5 Temperature dependence of the resistance of moderately insulating Be film in units of h/e^2 in zero field (circles) and in a perpendicular field of H = 8.4 T (triangles). Inset: Temperature dependence of the resistance of a similar Be film

.

metals. In particular, Tedrow and Meservey (Tedrow and Meservey, 1982) reported that, for each monolayer of Pt deposited on a 40 Å-thick Al film, the SOS scattering rate h/τ_{so} increased by 3.2 meV. Similarly, large SOS rates can be induced in Be films by coating them with Au (Wu *et al.*, 2006). The primary effect of SOS is to disrupt the spin rotation symmetry of the system, so that spin is no longer a good quantum number. However, conventional BCS superconductivity does not require spin rotation symmetry, therefore SOS has little effect on the zero field properties of the condensate. Nevertheless, the spin response of a superconductor, as probed by a parallel magnetic field, is much different in the presence of SOS. The most apparent ramification of SOS is a dramatic increase in the parallel critical field (Wu *et al.*, 2006). Thin superconducting Be films coated with 5 Å of Au can have a parallel critical field that is an order of magnitude larger that the Clogston-Chandresekhar limit. Naively, one would expect a similar SOS effect on the parallel pair-breaking field of localized Cooper pairs.

In Fig. 3.7 we compare the perpendicular and parallel-field MR of the Be/Au bilayers. The bilayers were formed by depositing varying Au thicknesses onto Be films. All of the depositions were made on fire polished glass substrates held at 84 K. First a Be film with thickness $\sim$ 18 Å was deposited at a rate of 1.4 Å/s, then a Au overlayer was deposited at 0.1 Å/s without breaking the vacuum. The data, which

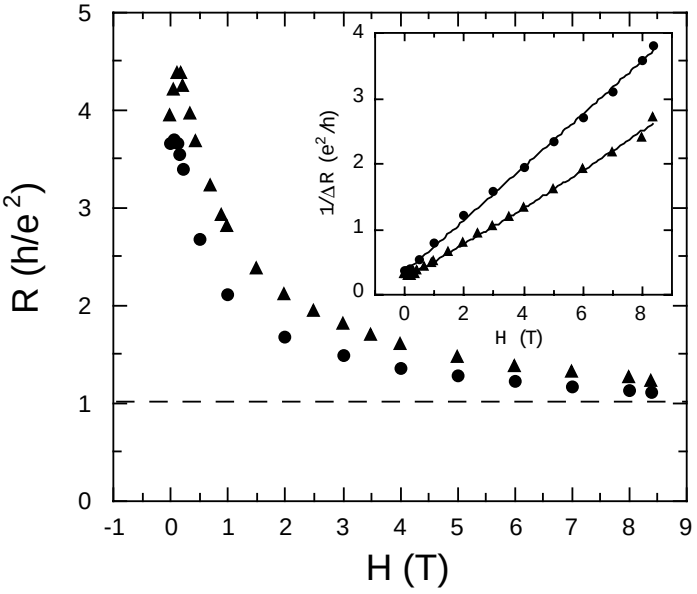

Fig. 3.6 Low temperature magnetoresistance of the films in Fig. 3.5 in units of h/e^2 at T = 50 mK, circles: main panel data, triangles: inset data. Note the saturation at $R \sim R_Q$. Inset: Linear behavior after subtracting off a saturation resistance of $0.85R_Q$, $\Delta R = R - 0.85$. The solid lines are provided as a guide to the eye

.

have been normalized by the zero field resistance, were taken at $400 - 500$ mK in order to circumvent the long, non-exponential relaxations that hinder measurements below 100 mK. The open circle symbols correspond to the uncoated 18 Å Be film which displays the previously reported low-field positive MR followed by a multi-fold negative MR (Butko *et al.*, 2000*a*; Butko *et al.*, 2000*b*). The dashed line near the x-axis in panel (b) of Fig. 3.7 corresponds to R_Q for the Be film. The MR appears to be asymptotic to R_Q, in accord with the high-field quantum metal phase (Butko and Adams, 2001). In contrast, the overall scale of the MR for the $d_{AU} = 0.3$ Å bilayer is somewhat diminished and almost completely quenched in the $d_{Au} = 0.6$ Å bilayer. Both of these samples have low temperature sheet resistances $R \gg R_Q$ and correlation energies $T_o \gg T$, as is the case for the uncoated film. Because of this we conclude that the MR is being modified by the spin-orbit scattering and not the lowering of T_o, for instance. Note that the MR peaks move to substantially higher fields with increasing Au coverage in the $d_{Au} = 0.0$, 0.3, and 0.6 nm curves. The $d_{Au} = 1.0$ curves display the largest MR anisotropy, but this may be a consequence of the fact that $T_o \sim T$ for this sample. Nevertheless, the high-field perpendicular MR is only weakly negative for the highest Au coverage bilayer, while the parallel MR maximum, if it exists, lies beyond 9 T.

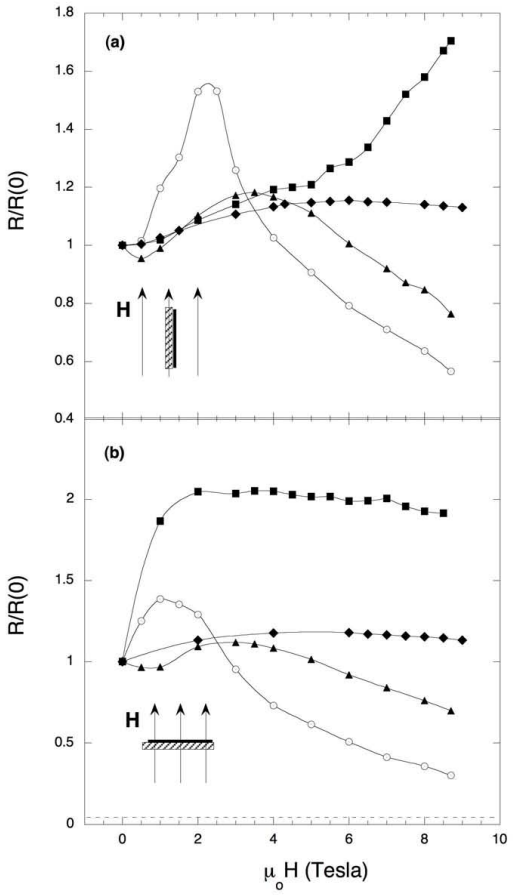

Fig. 3.7 The normalized resistance of the Be/Au films as a function of parallel (upper panel) and perpendicular magnetic field (lower panel). The $d_{Au} = 0.0$ curves were taken at 500 mK. The other curves were taken at 400 mK.

4

Summary and Zero Temperature Phase Diagram

The ground state properties of the Be films are most effectively summarized using the schematic phase diagram in Fig. 4.1. The x-axis measures the amount of disorder which we parameterize as $1/t$, where t is the film thickness. The y-axis is the applied magnetic field. In the limit of $1/t \rightarrow 0$ the films are 3-dimensional (3D). As the thickness is lowered, however, the 3D to 2D threshold is crossed, and the films become weakly metallic with a perturbative logarithmic increase in resistance with decreasing temperature and a perturbative logarithmic suppression of the DOS near the Fermi energy. Interestingly, Be also has a locally enhanced superconducting phase in the weakly metallic regime, shown in blue. The S-P transition occurs at the boundary between the rightmost portion of the superconducting (SC) dome and the weak metal phase. In the vernacular of the S-P formalism the weak metal phase above the dome is often referred to as the Pauli-limited normal state. The small arrow at the top of the dome shows how the phase boundary is modified in the presence of SOS.

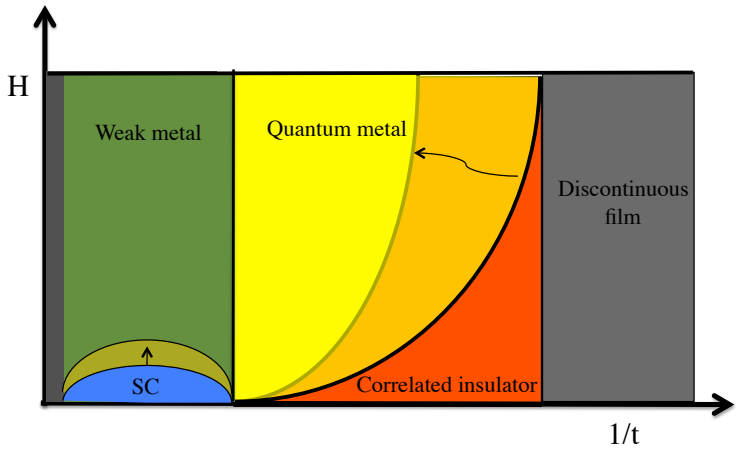

Fig. 4.1 Zero temperature phase diagram of a disordered thin film system with low spin-orbit scattering. The arrows in the diagram show how the phase boundaries are shifted in the presence of the spin-orbit scattering.

As the film thickness is decreased further the disorder increases and electron correlation effects begin to dominate the normal state transport properties. In this regime $R \rightarrow R_Q$ and states near the Fermi energy are rapidly depleted, signaling the emergence of the Coulomb gap and destruction of long range superconducting phase coherence. This zero-field S-I transition occurs between the blue and red portions of the phase diagram. There is now good evidence that localized Cooper pairs participate in this transition. Furthermore, anomalous ultra-large MR peaks are also seen in this region. The latter observation suggests that the phase diagram in Fig. 4.1 may be oversimplified near the zero-field S-I boundary. Further decreases in thickness at zero field result in films with $R \gg R_Q$. These films are correlated insulators, shown in red, and are characterized by a well defined Coulomb gap and Efros-Shklovskii hopping transport. The deeper one moves to the right in the correlated insulator region of the diagram the greater the correlation energy T_o becomes, until one eventually reaches the percolation threshold of the film, at which point it is no longer electrically continuous. This occurs at $t \sim 1$ nm in Be films. We have shown that the application of a magnetic field lifts the Coulomb gap thereby producing extremely large decreases in resistance at low temperatures. As the diagram in Fig. 4.1 indicates, we believe that this process eventually leads to a saturation in the resistance near R_Q even for films deep in the correlated insulator regime. This weakly temperature dependent, high field state is depicted in yellow and essentially behaves as a weak metal. Thus the yellow region in Fig. 4.1 describes films of varying disorder but with resistance near R_Q. The boundary between the quantum metal phase and the correlated insulator phase is sensitive to SOS in manner similar to that of the SC phase. The curved arrow depicts the effect of SOS on the correlated insulator - quantum metal boundary. This sensitivity to SOS suggests that localized Cooper pairs persist deep into the correlated insulator phase and that the primary effect of SOS scattering is to increase the Zeeman critical field of the localized Cooper pairs beyond the Clogston-Chandrashekar limit. The almost ideal morphological characteristics of Be films, along with the fact that Be undergoes a zero-field S-I transtion, lead us to believe that the general features of Fig. 4.1 are generic to low SOS, thin-film S-I systems.

Until very recently, the zero-field S-I transition in homogeneously disordered films was thought to be mediated by the destruction of the magnitude of the order parameter as one approached the transition from the clean limit. A general consensus had emerged that the convolution of $e - e$ interactions and disordered reduced the available normal state DOS to the point that a superconducting condensate was no longer sustainable, even at zero temperature, in critically disordered systems. However, as discussed in this and other chapters there is compelling new evidence that, though the order parameter indeed goes to zero at the S-I transition, local Cooper pairing occurs well into the insulating phase. This somewhat counter-intuitive scenario is made even more plausible by the fact that incoherent Cooper pairing is clearly evident in the Pauli-limited normal state of moderately disordered superconducting films. Hopefully future experiments will be able elucidate the relationship between incoherent pairing on the superconducting side of the S-I transition with localized Cooper pairing on the insulating side. Quantitative progress on this issue is a crucial ingredient to our ultimate understanding of underlying quantum nature of the S-I transition.

References

Abrahams, E., Anderson, P.W., Licciardello, D.C, and Ramakrishnan, T.V. (1979, Mar). *Phys. Rev. Lett.*, **42**(10), 673–676.

Adams, P. W. (2004). *Phys. Rev. Lett.*, **92**(6), 067003.

Adams, P. W. and Butko, V. Yu. (2000). *Physica B*, **284**, 673–674.

Adams, P. W., Herron, P., and Meletis, E. I. (1998). *Phys. Rev. B*, **58**(6), R2952–R2955.

Aleiner, I. L. and Altshuler, B. L. (1997). *Phys. Rev. Lett.*, **79**(21), 4242–4245.

Alexander, J.A.X., Orlando, T.P., Rainer, D., and Tedrow, P.M. (1985). *Phys. Rev. B*, **31**(9), 5811–5825.

Altshuler, B.L., Aronov, A.G., Gershenson, M.E., and Sharvin, Yu.V. (1987). *Sov. Sci. Rev. A*, **9**, 223.

Baturina, T.I., Strunk, C., Baklanov, M.R., and Satta, A. (2007). *Phys. Rev. Lett.*, **98**, 127003.

Baym, G. and Pethick, C. (1991). *Landau Fermi-Liquid Theory: Concepts and Applications*. John Wiley & Sons, New York.

Bergmann, G. (1983). *Phys. Rev. B*, **28**, 2914.

Butko, V.Yu. and Adams, P.W. (2001). *Nature*, **409**, 161.

Butko, V.Yu., DiTusa, J.F., and Adams, P.W. (2000*a*). *Phys. Rev. Lett.*, **85**, 162.

Butko, V. Y., Adams, P. W., and Aleiner, I. L. (1999). *Phys. Rev. Lett.*, **82**(21), 4284–4287.

Butko, V. Yu., DiTusa, J.F., and Adams, P.W. (2000*b*). *Phys. Rev. Lett.*, **84**, 1543.

Chandrasekhar, B. S. (1962). *Appl. Phys. Lett.*, **1**, 7–8.

Clogston, A. M. (1962). *Phys. Rev. Lett.*, **9**, 266–267.

Dynes, R.C., Garno, J.P., and Rowell, J.M. (1978). *Phys. Rev. Lett.*, **40**, 479.

Efros, A.L. and Shklovskii, B.I. (1975). *J. Phys. C*, **8**, L49.

Efros, A.L. and Shklovskii, B.I. (1984). *Electronic Properties of Doped Semiconductors*. Springer, New York.

Entin-Wohlman, O., Imry, Y., and Sivan, U. (1989). *Phys. Rev. B*, **40**, 8342.

Epstein, K., Goldman, A.M., and Kadin, A.M. (1983). *Phys. Rev. B*, **27**, 6685.

Fulde, P. (1973). *Adv. Phys.*, **22**, 667.

Gantmakher, V.F., Golubkov, M.V., Dolgopolov, V.T., Shashkin, A.A., and Tsydynzhapov, G.E. (2000). *Pis'ma Zh. Eksp. Teor. Fiz.*, **71**, 693. [JETP Lett. **71**, 473 (2000)].

Gantmakher, V.F., Golubkov, M.V., Dolgopolov, V.T., Tsydynzhapov, G.E., and Shashkin, A.A. (1998). *Pis'ma Zh. Eksp. Teor. Fiz.*, **68**, 337. [JETP Lett. **68**, 363 (1998)].

Gibson, G. A., Tedrow, P. M., and Meservey, R. (1989). *Phys. Rev. B*, **40**, 137.

Goldman, A. M. and Markovic, N. (1998). *Phys. Today*, **51**(11), 39.

Haviland, D.B., Liu, Y., and Goldman, A.M. (1989). *Phys. Rev. Lett.*, **62**, 2180.
Hebard, A.F. and Paalanen, M.A. (1990). *Phys. Rev. Lett.*, **65**, 927.
Hernandez, L. M., Bhattacharya, A., Parendo, Kevin A., , and Goldman, A. M. (2003). *Phys. Rev. Lett.*, **91**, 126801.
Hernandez, P. and Sanquer, M. (1992). *Phys. Rev. Lett.*, **68**, 1402.
Imry, Y. and Ovadyahu, Z. (1982). *Phys. Rev. Lett.*, **49**, 841.
J. M. Valles, Jr., Dynes, R.C., and Garno, J.P. (1992). *Phys. Rev. Lett.*, **69**, 3567.
Lee, P. A. and Ramakrishnan, T.V (1985, Apr). *Rev. Mod. Phys.*, **57**(2), 287–337.
Massey, J.G. and Lee, M. (1995). *Phys. Rev. Lett.*, **75**, 4266.
Matveev, K.A., Glazman, L.I., Clarke, P., Ephron, D., and Beasley, M.R. (1995). *Phys. Rev. B*, **52**, 5289.
Medina, E., Kardar, M., and Rangel, R. (1996). *Phys. Rev. B*, **53**, 7663.
Meservey, R. and Tedrow, P. M. (1976). *Phys. Lett. A*, **58**(2), 131–132.
Meservey, R., Tedrow, P. M., and Fulde, P. (1970). *Phys. Rev. Lett.*, **25**(18), 1270–&.
Mott, N.F. and Davis, G.A. (1979). *Electronic Processes in Non-Crystalline Materials*. Springer-Verlag, New York.
Nguyen, V.I., Spivak, B.Z., and Shklovskii, B.I. (1985). *Pis'ma Zh. Eksp. Teor. Fiz.*, **41**, 35. [JETP Lett. **41**, 42 (1985)].
Pichard, J.L., Sanquer, M., Slevin, K., and Debray, P. (1990). *Phys. Rev. Lett.*, **65**, 1990.
Sambandamurthy, G., Engel, L.W., Johansson, A., and Shahar, D. (2004). *Phys. Rev. Lett.*, **92**, 107005.
Shapir, Y. and Ovadyahu, Z. (1989). *Phys. Rev. B*, **40**, 12441.
Steiner, M.A., Boebinger, G., and Kapitulnik, A. (2005). *Phys. Rev. Lett.*, **94**, 107008.
Stewart, M.D., Yin, A., Xu, J.M., and J.M. Valles, Jr. (2007). *Science*, **318**, 1273.
Suzuki, T., Seguchi, Y., and Tsuboi, T. (2000). *J. Phys. Soc. Jpn.*, **69**(5), 1462–1471.
Tedrow, P.M., Kucera, J.T., Rainer, D., and Orlando, T.P. (1984). *Phys. Rev. Letts*, **52**(18), 1637.
Tedrow, P.M. and Meservey, R. (1982). *Phys. Rev. B*, **25**(1), 171.
Tedrow, P. M. and Meservey, R. (1979). *Phys. Rev. Lett.*, **43**(5), 384–387.
Tinkham, M. (1996). *Introduction to Superconductivity*. McGraw-Hill, New York.
White, A.E., Dynes, R.C., and Garno, J.P. (1985). *Phys. Rev. B*, **31**, 1174.
Wu, Wenhao and Adams, P. W. (1994). *Phys. Rev. Lett.*, **73**(10), 1412–1415.
Wu, Wenhao and Adams, P. W. (1995). *Phys. Rev. Lett.*, **74**(4), 610–613.
Wu, Wenhao, Goodrich, R. G., and Adams, P. W. (1995). *Phys. Rev. B*, **51**(2), 1378–1380.
Wu, X.S., Adams, P. W., and Catelani, G. (2006). *Phys. Rev. B*, **74**, 144519.